12-2017

Intermetallic structures with atomic precision for selective hydrogenation of nitroarenes

Yuchen Pei
Iowa State University and Ames Laboratory, peiyc@iastate.edu

Zhiyuan Qi
Iowa State University and Ames Laboratory, zhiyuan7@iastate.edu

Tian Wei Goh
Iowa State University and Ames Laboratory, jasongoh@iastate.edu

Lin-Lin Wang
Ames Laboratory, llw@ameslab.gov

Raghu V. Maligal-Ganesh
Iowa State University and Ames Laboratory, raghuv96@iastate.edu

See next page for additional authors

Intermetallic structures with atomic precision for selective hydrogenation of nitroarenes

Abstract
Bridging the structure-properties relationship of bimetallic catalysts is essential for the rational design of heterogeneous catalysts. Different from random alloys, intermetallic compounds (IMCs) present atomically-ordered structures, which is advantageous for catalytic mechanism studies. We used Pt-based intermetallic nanoparticles (iNPs), individually encapsulated in mesoporous silica shells, as catalysts for the hydrogenation of nitroarenes to functionalized anilines. With the capping-free nature and ordered atomic structure, PtSn iNPs show >99% selectivity to hydrogenate the nitro group of 3-nitrostyrene albeit with a lower activity, in contrast to Pt3Sn iNPs and Pt NPs. The geometric structure of PtSn iNPs in eliminating Pt threefold sites hampers the adsorption/dissociation of molecular H2 and leads to a non-Horiuti-Polanyi hydrogenation pathway, while Pt3Sn and Pt surfaces are saturated by atomic H. Calculations using density functional theory (DFT) suggest a preferential adsorption of the nitro group on the intermetallic PtSn surface contributing to its high selectivity.

Keywords
Intermetallic compounds, Platinum-tin alloy, 3-Nitrostyrene, Threefold site, Horiuti-Polany mechanism, Hydrogen dissociation

Disciplines
Materials Chemistry | Materials Science and Engineering | Physical Chemistry

Authors
Yuchen Pei, Zhiyuan Qi, Tian Wei Goh, Lin-Lin Wang, Raghu V. Maligal-Ganesh, Heather L. Macmurdo, Shiran Zhang, Chaoxian Xiao, Xinle Li, Franklin (Feng) Tao, Duane D. Johnson, and Wenyu Huang

Intermetallic Structures with Atomic Precision for Selective Hydrogenation of Nitroarenes

Yuchen Pei,[†‡] Zhiyuan Qi,[†‡] Tian Wei Goh,[†‡] Lin-Lin Wang,[‡] Raghu V. Maligal-Ganesh,[†‡] Heather L. MacMurdo,[†] Shiran Zhang,[§] Chaoxian Xiao,[†] Xinle Li,[†] Franklin (Feng) Tao,[§] Duane D. Johnson,[‡¥] and Wenyu Huang[*†‡]

†Department of Chemistry, Iowa State University, Ames, IA 50011, United States
‡Ames Laboratory, U.S. Department of Energy, Ames, IA 50011, United States
§Department of Chemical & Petroleum Engineering, Department of Chemistry, University of Kansas, Lawrence, Kansas 66045, United States
¥Department of Materials Science & Engineering, Iowa State University, Ames, IA 50011, United States

*Corresponding author. E-mail: whuang@iastate.edu

Abstract

Bridging the structure-properties relationship of bimetallic catalysts is essential for the rational design of heterogeneous catalysts. Different from random alloys, intermetallic compounds (IMCs) present atomically-ordered structures, which is advantageous for catalytic mechanism studies. We used Pt-based intermetallic nanoparticles (iNPs), individually encapsulated in mesoporous silica shells, as catalysts for the hydrogenation of nitroarenes to functionalized anilines. With the capping-free nature and ordered atomic structure, PtSn iNPs show >99% selectivity to hydrogenate the nitro group of 3-nitrostyrene albeit with a lower activity, in contrast to Pt_3Sn and Pt NPs. The geometric structure of PtSn iNPs in eliminating Pt threefold sites hampers the adsorption/dissociation of molecular H_2 and leads to a non-Horiuti-Polanyi hydrogenation pathway, while Pt_3Sn and Pt surfaces are saturated by atomic H. Calculations using density functional theory (DFT) suggest a preferential adsorption of the nitro group on the intermetallic PtSn surface contributing to its high selectivity.

Keywords
Intermetallic compounds, platinum-tin alloy, 3-nitrostyrene, threefold site, Horiuti-Polany mechanism, hydrogen dissociation

1. Introduction

Engineering catalytically active sites is critical to establish a molecular understanding of structure-property relationships, and thus guide the design of highly active and selective catalysts. Bimetallic alloys composed of noble metals are efficient catalysts for selective hydrogenations. However, correlating the atomic structures of alloy catalysts with their catalytic properties is challenging owing to the random arrangement of atoms in most alloy structures. Intermetallic compounds (IMCs) are special alloys featuring atomically-ordered and thermodynamically stable structures with defined stoichiometry, which render IMCs ideal platforms to study mechanisms of catalytic reactions in comparison to random alloys [1-3]. IMCs can manipulate the adsorption energy and geometry of reactants and intermediates that could vary catalytic pathways. Moreover, the addition of inexpensive metals to noble metal-based IMCs can efficiently utilize noble metals through a homogenous dilution. The isolation of noble metal sites can significantly improve the selectivity by suppressing over-hydrogenated products in many selective hydrogenation reactions [4-7]. Therefore, the synthetic development of intermetallic catalysts with homogeneous composition and structure

becomes essential for the bottom-up design of intermetallic catalysts and their mechanism studies. To improve the precision in the preparation of catalysts apart from the traditional wetness impregnation method, our group demonstrated a seeded-growth method and obtained series of Pt-based intermetallic nanoparticles (iNPs) individually encapsulated in mesoporous silica shells (PtM@mSiO_2, M = Sn, Zn, and Pb) [8-10]. These iNPs have well-defined intermetallic structure, precise composition, capping-free surface, and high thermal stability that provide an optimal platform to elucidate the unique catalytic properties of IMCs.

The selective hydrogenation of nitroarenes constitutes an important industrial process for the production of functionalized anilines widely used as pharmaceuticals, herbicides, and pigments [11]. The challenge of this reaction is to selectively hydrogenate the nitro group in the presence of other reducible/leaving groups (e.g., C=C, C=O, C≡N, and halides). Commercial synthesis of functionalized anilines requires a stoichiometric addition of reducing agents (i.e. Zn-NH_3 and $Na_2S_2O_4$) and generates excessive waste [12]. Nobel metal-based heterogeneous catalysts are thus developed for this reaction and used in an eco-friendly manner [9, 13-15]. Using alloys is an effective strategy to suppress noble metal ensembles and thus the over-hydrogenation capability of noble metals, which enhances their selectivity in hydrogenation reactions [16-18]. In regards of the atomically ordered IMCs, limited compositions have been reported as selective catalysts in comparison to a variety of alloys [19, 20]. It is intriguing if the high selectivity in the hydrogenation of nitroarenes can be extended to other IMCs, and further structural studies are essential to elucidate the origin of this high selectivity on IMCs with homogeneous compositions and well-defined structures.

Pt-containing IMCs have shown high activity and selectivity in selective hydrogenations [21-23], such as PtSn iNPs in the hydrogenation of furfural to furfuryl alcohol [8]. Herein, we report the selective hydrogenation of 3-nitrostyrene using PtM@mSiO_2 iNPs (M = Sn, Zn, and Pb). To tune the degree of Pt dilution by Sn, we synthesized PtSn and Pt_3Sn iNPs. Different from Pt and Pt_3Sn@mSiO_2, PtSn@mSiO_2 demonstrates >99% nitro hydrogenation selectivity due to the preferential adsorption of the nitro group on the intermetallic PtSn surface. The high selectivity is universal to various functionalized nitroarenes over PtSn@mSiO_2 and other PtM typed iNPs such as PtZn and PtPb iNPs. An abrupt drop in activity on PtSn@mSiO_2 was also observed in contrast to Pt and Pt_3Sn@mSiO_2, which cannot be explained solely by the decrease of Pt density on the surface. We conferred a non-Horiuti-Polanyi (HP) mechanism over intermetallic PtSn where hydrogenations proceed likely with molecular H_2 as opposed to atomic H. The variance of hydrogenation pathway is readily determined by the geometric structures of intermetallic PtSn because the elimination of threefold Pt sites on intermetallic PtSn inhibits H_2 dissociation [24-27]. This work exemplifies the relationship between intermetallic structures and their unique catalytic performance in heterogeneous catalysis.

2. Experimental

2.1 Synthesis of Pt_3M/PtM@mSiO_2 (M = Sn, Zn, and Pb)

In a typical synthesis of Pt_3M/PtM@mSiO_2 NPs, as-synthesized Pt@mSiO_2 seeds (containing 10 mg Pt, stored in methanol) and secondary metal precursor ($SnCl_2$•$2H_2O$, $Pb(CH_3COO)_2$•$3H_2O$, and $Zn(acac)_2$•xH_2O) were well dispersed in 80 mL tetraethylene glycol (TEG) via sonication (for Zn precursor, 45 mL oleylamine and 15 mL oleic acid was used). The reaction flask was sealed with a septum, and the solution was subjected to vacuum to remove methanol. Under argon protection, the mixture was heated to 280 °C and stayed for 2 h with vigorous stirring (350 °C was used for the synthesis of PtZn and Pt_3Zn). After allowing the solution to cool down to room temperature, 80 mL of acetone was added to the reaction solution. Pt_3M/PtM@mSiO_2 NPs were collected by centrifugation and washed with methanol 3 times. All Pt_3M/PtM@mSiO_2 NPs were calcined at 500 °C for 4 h to burn off organic remnants and reduced at specific temperatures in 10% H_2/Ar (total flow rate: 50 mL/min) to form the corresponding intermetallic phases.

PtSn and PtPb were reduced at 300 °C for 2 h. PtZn, Pt_3Zn, and Pt_3Sn were reduced at 600 °C for 6 h. The $Pt@mSiO_2$ control sample was treated with the same procedure as $PtSn@mSiO_2$. Alloy $PtSn_{0.3}@mSiO_2$ was used after washing and vacuum drying from the wet synthesis.

2.2 Catalytic evaluation

Typically, 1-2 mg catalysts, 50 mg 3-nitrostyrene and 2 mL toluene were mixed in a 5 mL vial. 20 mg xylene was then added as an internal standard. The vial was placed in a Parr 4740 high-pressure/high-temperature vessel. After exchanging the atmosphere with H_2, the high-pressure vessel was charged with 20 bar H_2 and maintained at 80 °C with a stirring speed set at 1200 rpm for the reaction. The products after the reaction were diluted and analyzed by an Agilent 6890N/5975 gas chromatograph mass spectrometer (GC-MS) equipped with an HP-5ms capillary column (30 m × 0.25 mm × 0.25 μm) and a flame ionization detector (FID). For kinetic studies, the vial was placed back into the high-pressure vessel and charged with high-pressure H_2 after sampling at atmospheric pressure.

2.3 Characterization

Powder X-ray diffraction (PXRD) patterns of the samples were acquired by a STOE Stadi P powder diffractometer using Cu K_α radiation (40 kV, 40 mA, λ = 0.1541 nm). For ambient pressure X-ray photoelectron spectroscopy (AP-XPS) analysis, all samples were dispersed in ethanol and then dropped on pyrolytic graphite. The reduction treatments to all samples were carried out in an incorporated high-pressure cell in the vacuum chamber of the AP-XPS, in which 0.2 Torr H_2 was introduced at different temperatures to study the surface composition of the $PtSn@mSiO_2$. After the treatment, H_2 was purged out, and the sample was taken out to a manipulator in ultrahigh vacuum for AP-XPS analysis. A flux of low energy electrons (8.5 eV, 60 mA) generated by a flood gun was used for each analysis to remove the surface charging effects due to the existence of $mSiO_2$ shell. All spectra were calibrated by Pt $4f_{7/2}$ at 71.2 eV. High resolution transmission electron microscopy (HRTEM), high-angle annular dark field scanning TEM (HAADF-STEM), and elemental mapping analysis were investigated using a Tecnai G2 F20 electron microscope equipped with an energy-dispersive X-ray spectroscopy (EDS) detector (Oxford INCA EDS) and a Titan Themis 300 probe corrected TEM with a Super-X EDS detector. The actual metal loadings in the catalysts were measured by inductively coupled plasma-mass spectroscopy (ICP–MS) (X Series II, Thermo Scientific). Diffuse reflectance infrared Fourier transform spectroscopy (DRIFTS) was conducted using an Agilent Cary 670 Fourier transform infrared spectroscopy equipped with a linearized HgCdTe (MCT) detector, a Harrick diffuse reflectance accessory, and a Praying Mantis high-temperature reaction chamber. CO was used as the probe molecule, and 10-20 wt.% sample was diluted with KBr. H_2/D_2 exchange experiments were conducted under ambient pressure using H_2/D_2 = 10/10 mL/min as the feed gas, where $H_2/HD/D_2$ signals were monitored using a mass spectrometer (Agilent 5975). The cyclic voltammetry (CV) curves were measured using a potentiostat (VSP-300, Bio-Logic Science Instruments). 5 mg catalysts were added in 2 mL hydrazine hydrate (78-82%) for overnight to remove the insulating $mSiO_2$ shell. To support the released metal NPs, certain amount of active carbon was added at the beginning of etching to achieve ~10 wt.% Pt loading. After washing with water for 3 times, etched catalysts were dispersed in a mixture of H_2O:isopropanol:5% Nafion solution (4:1:0.025) to prepare a 0.5 mg/mL ink. 20 μL catalyst ink was transferred onto a rotational ring-disk working electrode (RRDE, 5 mm diameter). A platinum wire and a saturated Ag/AgCl electrodes were used as the counter and the reference electrodes, respectively. The experiment was conducted in 0.1 M $HClO_4$ under an argon atmosphere with a scan speed of 50 mV/s. The water used in experiments was Millipore ultrapure water (18.2 MΩ•cm).

2.4 Density Functional Theory (DFT) calculations

All DFT calculations have been carried out with PBE for exchange-correlation functional, a plane-wave basis set and projector augmented wave method as implemented in the Vienna Atomic Simulation Package (VASP). The Pt(111) surface is modeled as a three-layer slab with a surface supercell of ($2\sqrt{3}\times3$). The

PtSn(11$\bar{2}$0) surface is modeled as a four-layer slab with a surface supercell of (2×2). Various flat and tilt configurations with different molecular orientations of 3-nitrostyrene on the surfaces have been tried to search for the most stable adsorption configurations on the surfaces. All the atoms except for the bottom two layers in the slab (fixed at bulk positions) are relaxed till the absolute values of forces are below 0.02 eV/Å. A kinetic energy cutoff of 400 eV for the plane wave basis set and a (5×5×1) *k*-point mesh with a Gaussian smearing of 0.05 eV have been used.

3. Results and Discussion

Intermetallic PtM@mSiO_2 (M = Sn, Zn, and Pb) and Pt_3M@mSiO_2 (M = Sn and Zn) were prepared by following a "ship-in-a-bottle" strategy [8]. These iNPs were calcined at 500 °C to completely remove capping agents and reduced at temperatures of 300 or 600 °C to form the corresponding intermetallic phases. Figure S1 in the Supporting Information shows the representative TEM images of these iNPs. Even after 600 °C reductions, all iNPs were isolated and well encapsulated within the mSiO_2 shell, which highlights the robust nature of the mSiO_2 shell against the aggregation of the encapsulated iNPs. Our previous studies demonstrated that this ship-in-a-bottle strategy can maintain a precise control of the secondary metals, and the growth of the bimetallic cores are facilitated by the etching of the inner interface of mSiO_2 shells likely by the ion species produced during the TEG reduction [9]. The mSiO_2 shells have an average pore size of ca. 2.5 nm, which allows the free access of small organic molecules, such as furfural and nitrobenzene [8, 9]. There iNPs are single crystals with well-ordered structures as shown in the HRTEM images (Figure 1a, f, and S1). The measured lattice distances correspond well with specific crystal facets associated with the corresponding intermetallic phases. We also acquired PXRD patterns to confirm the formation of the desired intermetallic phases for all iNPs (Figure S2). The exact ratios of Pt to the secondary metal M are in good agreement with the theoretical values measured via ICP-MS (Table S1).

We evaluated the catalytic properties of these iNPs in the selective hydrogenation of 3-nitrostyrene. 3-nitrostyrene is composed of a nitro group and a vinyl group. The major hydrogenation products range from desired 3-aminostyrene (**1**), undesired 3-ethylnitrobenzene (**2**) and over-hydrogenated 3-ethylaniline (**3**). It is challenging to exclusively hydrogenate nitro group in the presence of more reducible C=C group over Pt-based catalysts. One effective strategy to fulfill the high selectivity in hydrogenating nitro group is to downsize Pt contiguous sites that can suppress C=C hydrogenation [16]. The addition of secondary metals in many alloys can dilute Pt contiguous sites and modify the adsorption geometry of 3-nitrostyrene on bimetallic surfaces. DFT calculation suggests that the catalytic mechanism for reducing nitroarenes over these bimetallic alloys is the preferential adsorption of nitro group on the isolated Pt sites. It is thus reasonable to hypothesize from the geometric consideration that eliminating Pt contiguous sites is essential and likely universal to achieve a high selectivity to the hydrogenation of the nitro group over Pt-containing bimetallic catalysts.

Even though Pt-based alloys are selective for reducing nitroarenes, inconsistent results have been reported [28-31]. This ambiguous catalysis on bimetallic alloys is likely due to their random geometry that cannot ensure the elimination of contiguous noble metal sites on the surface, and thus leads to the low nitro hydrogenation selectivity. Proper IMCs with ordered structure could completely remove the contiguous noble metal sites and lead to high selectivity in nitro hydrogenation. However, only limited compositions (PtZn, PtGa, and RhIn) have been studied over ordered IMCs [19, 20, 29]. In this work, we endeavor to utilize more structurally ordered and thermodynamically stable IMCs to study the structure-property relationship in selective hydrogenations, especially the effect of eliminating Pt contiguous sites. We choose PtSn iNPs as a model because previous work has shown that bimetallic PtSn alloys/H-WO_3 exhibited 75% selectivity to 3-nitrostyrene hydrogenation in comparison to Pt controls [28]. PtSn with 1:1 atomic ratio can

form a NiAs-type IMC with hexagonal *hP*4 cells. We examined the low index facets of intermetallic PtSn(11$\bar{2}$0), (0001), and (11$\bar{2}$1) facets that are most likely present in spherical iNPs (Figure S3) [32-35]. On all these facets, contiguous Pt sites (specifically threefold sites) are eliminated due to the highly ordered nature of iNPs. Based on these reasons, intermetallic PtSn@mSiO$_2$ is a promising model to study the structure-property relationship in the selective hydrogenation of 3-nitrostyrene. As a comparison, we also prepared Pt_3Sn iNPs that contain Pt contiguous sites on their surfaces.

To visualize the homogeneous structures of our Pt_3Sn@mSiO$_2$ and PtSn@mSiO$_2$, HAADF-STEM images were acquired as shown in Figure 1. Figure 1b-c depict the *P6$_3$/mmc* PtSn iNPs oriented in the [010] direction, consistent with the uniform hexagonal FFT diffraction pattern. The lattice spacing of 0.416 nm agrees with the theoretical value of the PtSn(10$\bar{1}$0) facet. Figure 1g-h show the *Pm*$\bar{3}$*m* Pt_3Sn along [011] orientation, which correlates with the distorted hexagonal FFT diffraction pattern. As illustrated in Figure S3, the ideal Pt_3Sn(110) is arranged with staggered Pt chains and alternating Pt/Sn chains. This arrangement is seen in Figure 1h when scanning the inner areas of Pt_3Sn iNPs (Pt chains are observed as brighter dots, and Pt/Sn chains are slightly darker) [36]. The lattice spacing was measured as 0.285 nm, conforming to the theoretical values of the Pt_3Sn(110) facet. The elemental mappings of PtSn and Pt_3Sn iNPs are also listed (Figure 1e and 1g, and both PtSn and Pt_3Sn demonstrate the evenly distributed Pt and Sn through the respective iNPs.

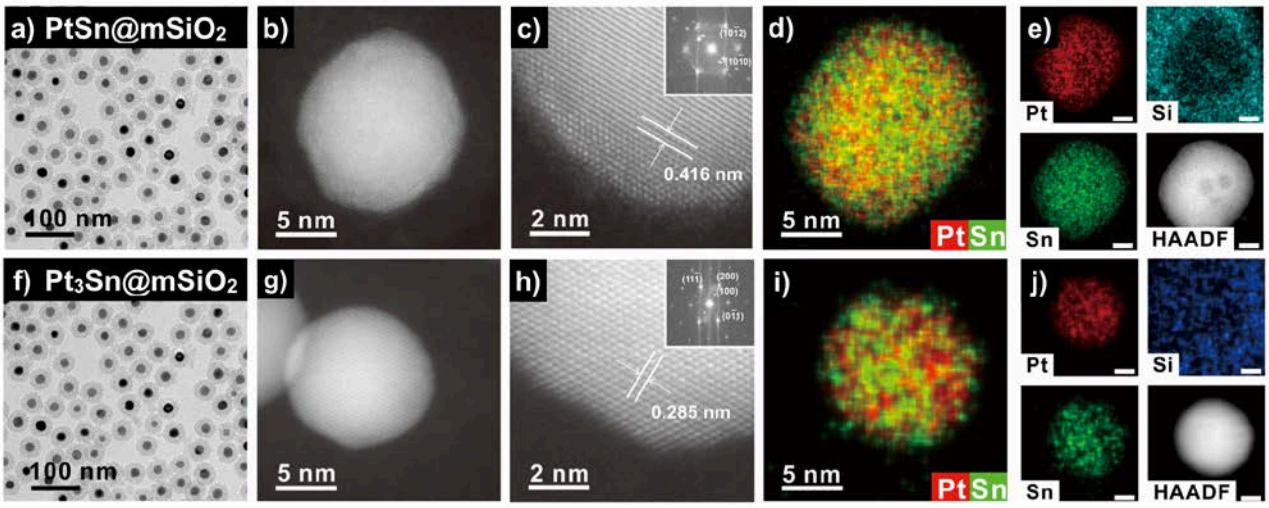

Figure 1. HRTEM and HAADF-STEM images of a-c) PtSn@mSiO$_2$, and f-h) Pt_3Sn@mSiO$_2$; insets in c) and h) are, respectively, fast Fourier transform (FTT) patterns from [0001] direction for PtSn@mSiO$_2$ and [110] direction for Pt_3Sn@mSiO$_2$; and elemental mappings of d-e) PtSn@mSiO$_2$, and i-j) Pt_3Sn@mSiO$_2$.

The catalytic performance of intermetallic PtSn@mSiO$_2$ in the selective hydrogenation of 3-nitrostyrene is summarized in Table 1. PtSn@mSiO$_2$ shows a significantly high selectivity to desired 3-aminostyrene **1** (>99%). To prove that both high conversion and selectivity can be achieved without over-hydrogenation, we extended the reaction time to 12 h after obtaining a full conversion. The byproducts (**2** and **3**) were still not detected, which proves the remarkable nitro hydrogenation selectivity of intermetallic PtSn. To further investigate how intermetallic geometry can impact the selectivity, we evaluated Pt@mSiO$_2$ and Pt_3Sn@mSiO$_2$. Intermetallic compounds typically have discrete stoichiometric compositions with crystal structures, setting them apart from those random alloys with tunable compositions and randomly arranged constituent atoms. Intermetallic Pt_3Sn@mSiO$_2$ has the Cu_3Au-type structure (*cP4* cells) with face-centered cubic (*fcc*) packing of Pt and Sn atoms [37, 38], which is similar to the structure of monometallic *fcc* Pt but differs significantly from hexagonal *hP4* PtSn. Pt@mSiO$_2$ and Pt_3Sn@mSiO$_2$ demonstrate higher activity

with respective 50- and 21-fold faster reaction rates compared to PtSn@mSiO$_2$. However, Pt@mSiO$_2$ directs the reaction to undesired C=C hydrogenation product **2** and over-hydrogenated product **3**. Although Pt$_3$Sn@mSiO$_2$ gives 40.4% selectivity to the hydrogenation of the nitro group (**1**) at the initial stage, this selectivity could not be maintained and rapidly shifted to over-hydrogenated product **3**. These catalysis results prove that PtSn@mSiO$_2$ is unique in its' high selectivity to the hydrogenation of the nitro group in 3-nitrostyrene. We subsequently investigated the scope of PtSn@mSiO$_2$ in the hydrogenation of nitroarenes with bromo, iodo, formyl and methoxy groups (Table 2). High selectivities to their corresponding functionalized anilines were achieved, demonstrating the general applicability of PtSn iNPs in the hydrogenation of various nitroarenes.

Table 1. Selective hydrogenation of 3-nitrostyrene over Pt NPs and Pt-based iNPs.[a]

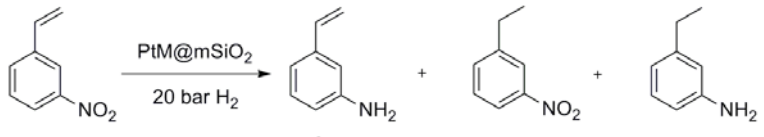

Entry	Catalyst	Time (h)	Rate [b] (g g_{Pt}^{-1} h^{-1})	TOF [c] (mol mol_{Pt}^{-1} h^{-1})	Conversion (%)	Selectivity		
						1	**2**	**3**
1	Pt@mSiO$_2$	0.16	471.4	9491	18.2	—	23.8	76.2
		1.0			99.2	—	2.0	98.0
2	PtSn@mSiO$_2$	6			40.8	>99	—	—
		9	9.3	676	>99	>99	—	—
		12			>99	>99	—	—
3	Pt$_3$Sn@mSiO$_2$	0.16	201.1	9274	62.2	40.4	—	59.6
		1			>99	—	—	>99
4	PtZn@mSiO$_2$	12	0.93	—	31.1	>99	—	—
5	Pt$_3$Zn@mSiO$_2$	1			76.5	88.8	—	11.2
		3	101.1	—	>99	88.9	—	11.1
		6			>99	37.9	—	62.1
6	PtPb@mSiO$_2$	12	5.0	—	97.5	>99	—	—

a. Reaction condition: 1 mg catalyst, 50 mg 3-nitrostyrene, 20 mg xylene as internal standard, 2 mL toluene as solvent, 80 ºC, and 20 bar H_2; b. Reaction rates were calculated at the conversion less than 20%, and Pt loadings were measured by ICP-MS; c. Turnover frequency (TOF) values were calculated based on specific Pt dispersions measured by CO chemisorption (6.5% for Pt@mSiO$_2$, 1.8% for PtSn@mSiO$_2$ and 2.8% for Pt$_3$Sn@mSiO$_2$).

Table 2. Selective hydrogenation of substituted nitroarenes over PtSn@mSiO$_2$ iNPs.[a]

Entry	Substrate	Product	Time (h)	Conversion (%)	Selectivity (%)
1	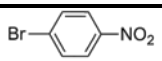	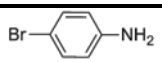	12	84.6	>99
2	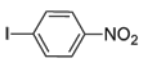	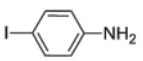	18	18.5	>99
3	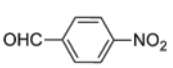	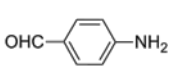	9	>99	>99
4	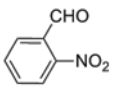	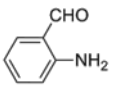	9	>99	76.3 [b]

5		18	31.2	> 99

a. Reaction condition: 1 mg catalyst, 0.4 mmol nitroarenes, 20 mg xylene as internal standard, 2 mL toluene as solvent, 80 ºC, and 20 bar H_2; b. Selectivity includes the partially intra-condensation product with incomplete reduced hydroxylamino group and formyl group.

It is intriguing to explore how the specific intermetallic structures in Pt-Sn systems can result in different catalytic behavior. To characterize the surface properties of intermetallic PtSn and Pt_3Sn, we conducted ambient pressure X-ray photoelectron spectroscopy (AP-XPS) with *in situ* reductions to study the surface evolution of catalysts when exposed to a reducing atmosphere at different temperatures. The catalysts were pre-calcined at 500 ºC and reduced at proper temperatures to form intermetallic phases (300 ºC for PtSn and 600 ºC for Pt_3Sn), which have been denoted as fresh samples. AP-XPS spectra in Figure 2 illustrates the surface composition for PtSn@mSiO_2 and Pt_3Sn@mSiO_2. High reduction temperatures are beneficial to induce the formation of metallic Sn and decrease the concentration of surface SnO_x species. Meanwhile, Pt majorly remains in the metallic state. The Pt/Sn atomic ratios of PtSn@mSiO_2 in fresh, 300, and 500 ºC reduced samples are 0.91, 0.91 and 0.94, respectively. These similar Pt/Sn atomic ratios indicate the relatively stable surface composition of intermetallic PtSn under a reducing atmosphere up to 500 ºC. Fresh Pt_3Sn@mSiO_2 have Pt/Sn atomic ratios of 2.78, which increases to 3.31 and 3.21 after *in situ* reductions at 300 and 500 ºC. A higher reduction temperature can introduce a slight segregation of Pt to the surface of Pt_3Sn iNPs. Except for the native Pt threefold sites on Pt_3Sn (111) (Figure S3b), the Pt-rich surface can contain more contiguous Pt sites speeding the over-hydrogenation pathways. The AP-XPS results support that the 300 ºC reduction for PtSn and 600 ºC reduction for Pt_3Sn can maintain their surface composition closed to their respective theoretical values. The AP-XPS results demonstrate that both surfaces of PtSn and Pt_3Sn iNPs closely reflect their bulk stoichiometric composition.

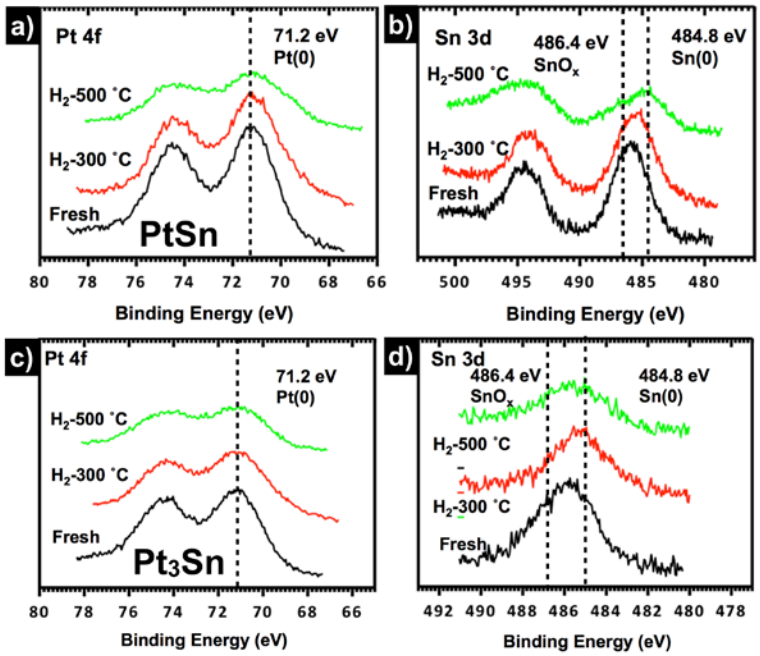

Figure 2. AP-XPS spectra of a) Pt 4f, b) Sn 3d in PtSn@mSiO_2, and c) Pt 4f, and d) Sn 3d in Pt_3Sn@mSiO_2.

With the atomically ordered intermetallic Pt_3Sn and PtSn, we attribute the dramatically diverse catalytic pathways of Pt, Pt_3Sn, and PtSn to their surface structures. Previous DFT calculations showed that Pt(111), Pt_3Sn(111), and PtSn(11$\bar{2}$0) hold the lowest surface energies [8, 39]. As shown in Figure 3a-c and S3, both Pt(111) and Pt_3Sn(111) contain contiguous Pt threefold sites [40]. PtSn(11$\bar{2}$0) only presents bridge Pt sites,

where the staggered Sn atoms disrupt the Pt threefold geometry. To further probe the surface Pt arrangement, we employed a CO-DRIFTS study for Pt, Pt_3Sn, and PtSn as shown in Figure 3d. Two major absorption peaks were observed in regions of 2050-2070 cm^{-1} and 1850-1870 cm^{-1} on Pt and $Pt_3Sn@mSiO_2$. The first intense peak is ascribed to atop CO linearly adsorbed on a single Pt atom, and the weak peak corresponds CO adsorbed over the bridge Pt sites [41]. Pt and Pt_3Sn have similar CO atop adsorption at ~ 2070 cm^{-1} [42], corresponding to their abundance of Pt threefold sites with a strong affinity to CO [43, 44]. The atop CO absorption shifts to low wavenumber region over the PtSn iNPs due to the electron donation from Sn to Pt [45]. However, the reduced CO dipole-dipole coupling effect cannot be completely ruled out. The addition of Sn in PtSn also shows a significant suppression of the bridge CO peak compared to Pt/Pt_3Sn, demonstrating that PtSn has different bridge Pt sites likely due to the interruption of the staggered Sn atoms. The intensity decrease of bridge CO and the peak shift of atop CO illustrate the decrease of Pt threefold sites (Pt>Pt_3Sn>>PtSn). Correlating CO-FTIR results to the catalytic activities, the reaction rate of $Pt@mSiO_2$ progresses 2- and 50-fold faster than $Pt_3Sn@mSiO_2$ and $PtSn@mSiO_2$. We also normalized the reaction rate to the accessible Pt sites by Pt dispersion. The TOF of $PtSn@SiO_2$ is still 14-fold less than that of $Pt@mSiO_2$. The TOF of $Pt_3Sn@mSiO_2$ (9274 h^{-1}) is close to that of $Pt@mSiO_2$ (9491 h^{-1}), confirming the catalytically identical Pt threefold sites on these two catalysts. The decreasing activity (Pt>Pt_3Sn>>PtSn) is consistent with the reduction of Pt threefold sites.

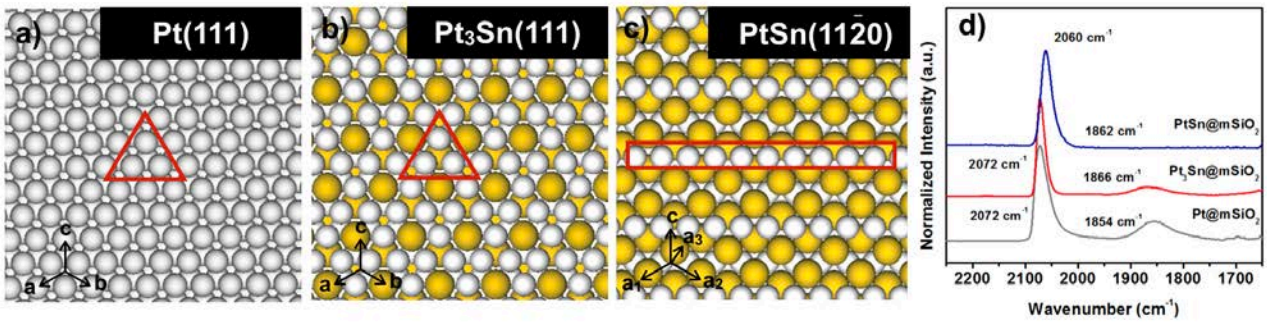

Figure 3. Ideal atomic geometry of a) Pt(111), b) Pt_3Sn(111), c) PtSn(11$\bar{2}$0), where Pt (grey spheres) and Sn (brown spheres) are indicated; d) DRIFTS spectra of $Pt@mSiO_2$, $Pt_3Sn@mSiO_2$, and $PtSn@mSiO_2$ using CO as the probe molecule. Pt 3-fold sites (red triangle in a and b) and Pt bridge sites (red rectangle in c) are marked.

The Pt threefold site is critical for the dissociative adsorption of H_2 molecules. The elimination of Pt threefold sites on intermetallic PtSn inhibits the H_2 adsorption/dissociation to form atomic H species, which hinders the activity in hydrogenation reactions using molecular H_2 [24, 26, 46, 47]. To validate the different behaviors of H_2 adsorption/dissociation on Pt and intermetallic PtSn, we employed H^+ electro-reduction, H_2 chemisorption, and H/D exchange experiments. The CV scans of intermetallic $PtSn@mSiO_2$ (after removing $mSiO_2$ shell) in 0.1 M $HClO_4$ show flat features from -0.25 to 0.15 V (vs Ag/AgCl). H^+ electro-reduction ($2H^+ \leftrightarrows H_2$) is clearly observed over Pt/Vulcan and $Pt@mSiO_2$ (-0.2-0 V in Figure S4) [48]. The two tails (-0.25 V) in the forward/backward scan on $Pt@mSiO_2$ demonstrate the adsorption and desorption of H_2 [49]. However, only H_2 desorption tail during the backward scan was observed over intermetallic $PtSn@mSiO_2$ sourced from the reduction of H^+. The absence of H_2 adsorption tail in the forward scan indicates a weak H_2 adsorption over PtSn in the liquid phase at room temperature. Negligible chemisorbed H_2 was observed on intermetallic $PtSn@mSiO_2$ either, similar to a previous report on alloy Sn/Pt (111) [25]. H/D exchange results further revealed the dramatically higher temperature (150 ^oC) required for H_2/D_2 exchange on $PtSn@mSiO_2$, compared to $Pt@mSiO_2$ (25 ^oC). This inability of H_2/D_2 dissociation has also been reported over intermetallic PtGe [50] and $PtSn/SiO_2$ [51]. Therefore, it is seen that intermetallic PtSn is ineffective at adsorption and dissociation of H_2. We thus propose that the hydrogenation on intermetallic

PtSn could largely proceed in a non-Horiuti-Polanyi (HP) pathway where molecular H_2 directly participates in the hydrogenations. Although the HP pathway involving atomic H is well-accepted on precious metals with a nearly barrierless H_2 dissociation [52], some catalysts have been reported with obstacles to breaking H-H bonds [53, 54]. Here, the intermetallic PtSn is exemplified as an exception to the traditional HP pathway in hydrogenations where a deficiency of atomic H was induced as a consequence of the elimination of Pt threefold sites. We endeavor to demonstrate that the physical state of H_2 can play important roles in hydrogenations, which has not been given significant emphasis.

Comparative DFT studies of the adsorption of 3-nitrostyrene on Pt(111) vs. PtSn(11$\bar{2}$0) were also performed to elucidate the origin of the nitro selectivity. On Pt(111) as shown in Figure 4a, 3-nitrostyrene prefers to adsorb in a flat configuration with both the center of the benzene ring and the vinyl group sitting on Pt bridge sites. This flat configuration maximises the number of C=C bonds interacting with the neighboring Pt bridge sites, while the nitro group is tilted away from the surface, which agrees with early DFT studies [55]. The strong band hybridization between Pt *d* and C *p* orbitals gives an adsorption energy of -2.08 eV. In contrast, on PtSn(11$\bar{2}$0) in Figure 4b without the contiguous Pt sites, the flat adsorption configuration is not preferred anymore, and the band hybridization between Pt *d* and C *p* orbitals becomes much weaker due to charge transfer from Sn to Pt that lowers the Pt *d*-band center [8]. Additionally, 3-nitrostyrene prefers to adsorb in a vertical configuration with the two O atoms in the nitro group sitting on top of Sn atoms. The interaction is mostly of ionic character with a charge transfer from Sn to O, resulting in a weak adsorption energy of -0.58 eV. We also varied the geometry of 3-nitrostyrene molecules on Pt(111) and PtSn(11$\bar{2}$0) facets to accommodate the contact of the benzene ring, C=C, and $–NO_2$ groups on these two facets as shown in Figure S5. Pt(111) facet gives the adsorption energy of -2.08, -1.16 and -0.19 eV for the respective benzene ring, C=C and $–NO_2$ group. Due to the straight-up geometry of the 3-nitrostyrene molecule on PtSn(11$\bar{2}$0), the adsorption energy of C=C and $–NO_2$ group was calculated as -0.12 and -0.58 eV. Such distinctively different adsorption configurations mean that the vinyl group is more accessible to the hydrogenation on Pt(111) or surfaces with contiguous Pt sites, while the nitro group can be hydrogenated selectively on PtSn(11$\bar{2}$0). These different adsorption geometries of 3-nitrostyrene on Pt(111) and PtSn(11$\bar{2}$0) explain the observed selectivity difference [19, 55, 56].

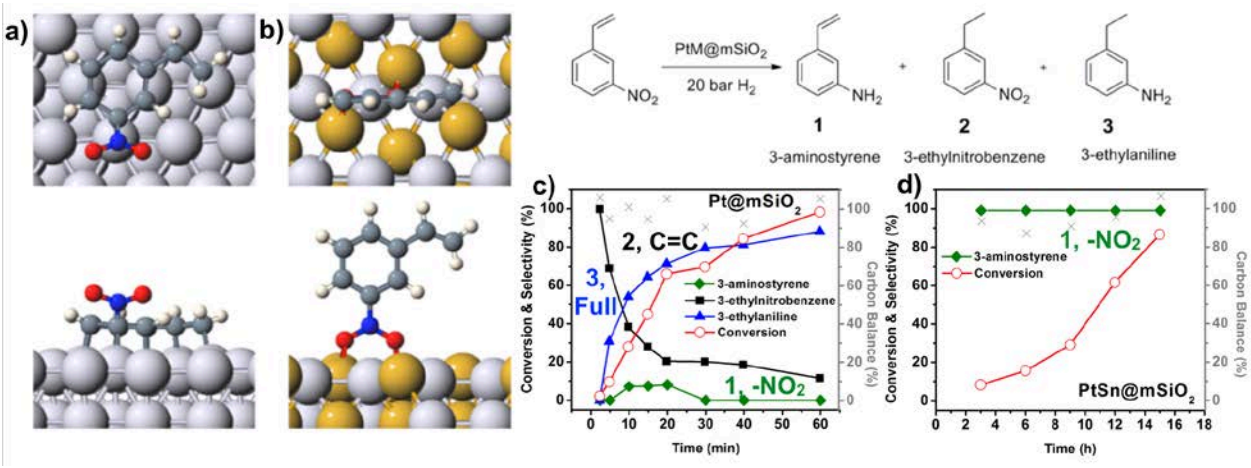

Figure 4. Most preferred adsorption configuration for 3-nitrostyrene: a) flat on Pt(111) and b) vertical on PtSn(11$\bar{2}$0) surfaces. Large grey (brown) spheres are Pt (Sn) atoms in the surfaces; small gray, blue, red and white spheres are C, N, O and H atoms in 3-nitrostyrene. The top (bottom) panel is the top (side) view. c-d) product distribution of 3-nitrostyrene hydrogenation over c) $Pt@mSiO_2$ and d) $PtSn@mSiO_2$.

We summarized the kinetic studies and product selectivity in Figure 4c-d and S6. In the liquid phase, H_2 molecules need to dissolve in the solvent and then contact catalytic surfaces to initiate reactions. To better evaluate the relationship between intermetallic catalysts and their catalysis, the dissolution factor of H_2 should be investigated. We acquired a volcano-shaped dependence between TOFs and H_2 pressure for both Pt@mSiO$_2$ and PtSn@mSiO$_2$ (Figure S6). Within the H_2 pressure ranging from 1-10 bar for Pt@mSiO$_2$ and 1-20 bar for PtSn@mSiO$_2$, a positive dependence was observed indicating that the H_2 dissolution kinetically controls the reaction. A negative dependence was observed with the further increase of the H_2 pressure. Later kinetic discussion is based on the results at the high-pressure region. For Pt@mSiO$_2$, the hydrogenation of 3-nitrostyrene was not highly dependent on either substrate concentration (168-503 mM, 20 bar H_2, slope = 0.08) or H_2 pressure (10-40 bar, 160 mM, slope = −0.43), which can be attributed to the strong adsorption of 3-nitrostyrene molecules over the Pt surface as revealed by the DFT calculation. Figure 4c shows the product distributions over Pt@mSiO$_2$ for the hydrogenation of 3-nitrostyrene. We noticed that vinyl groups readily underwent faster hydrogenation giving 3-ethylnitrobenzene (**2**) in comparison to the hydrogenation of nitro groups giving 3-ethylaniline (**3**) over Pt@mSiO$_2$, experimentally confirming the flat adsorption geometry of 3-nitrostyrene and the slower catalytic hydrogenation kinetics of tilted nitro groups. The slightly negative dependence of H_2 reaction order indicates the slight competition of atomic H and 3-nitrostyrene molecules on active Pt sites.

Looking into intermetallic PtSn@mSiO$_2$, a similar non-dependence of 3-nitrostyrene (168-503 mM, 20 bar H_2, slope = 0.02) was observed. However, unlike pure Pt, DFT calculations conjecture a weak adsorption of 3-nitrostyrene vertically adsorbed on the intermetallic PtSn surface due to the elimination of contiguous Pt sites. The vertically adsorbed 3-nitrostyrene has a weak interaction with PtSn (-0.58 eV) through the nitro group, and the vinyl group largely deviates from the PtSn surface. Such weak adsorption of nitro groups also agrees on the catalytic preference that the non-HP pathway of hydrogenation is more preferential on a polar group with a weak adsorption, which has been suggested by the previous DFT calculations for the selective hydrogenation of acrolein over Au sites [57]. When increasing the H_2 pressure, we observed a steeply negative dependence of H_2 pressure (20-40 bar H_2, 168 mM, slope = −1.25), indicating that a higher H_2 concentration has an adverse impact on the reaction. Noting that H_2 molecules are not likely dissociative over the intermetallic PtSn surface, such impedance can be explained solely by a significant competitive adsorption of both weakly adsorbed molecular H_2 and 3-nitrostyrene. It is worth to note that PtSn@mSiO$_2$ is almost inactive under 5 bar H_2, and thus a switch-on H_2 pressure is critical to initiate the reaction through the non-HP pathway. In addition to the geometry of 3-nitrostyrene, we performed control experiments using either styrene or nitrobenzene as substrates to evaluate the hydrogenation of single vinyl and nitro groups over PtSn@mSiO$_2$. The TOFs of nitrobenzene and styrene were relatively close, at 194 and 150 h^{-1} respectively when 40 bar H_2 was employed. When both styrene and nitrobenzene were present in one-pot to test the competitive hydrogenation in the presence of the same 40 bar H_2, intermetallic PtSn@mSiO$_2$ can only hydrogenate nitrobenzene (TOF = 61 h^{-1}), while largely hampered the hydrogenation of styrene. These results confirmed the preferential adsorption of nitro groups over vinyl groups in intermetallic PtSn@mSiO$_2$, which is consistent with the molecular adsorption geometry from DFT calculations. Similar catalytic trends were also reported by using single site-based Pt/FeO$_x$ catalysts [16], confirming that the absence of contiguous Pt in the well-ordered structure of intermetallic PtSn@mSiO$_2$ is beneficial to the selective hydrogenation of the nitro group.

Confirming that the structures of Pt, Pt_3Sn, and PtSn can alter the catalytic pathway and selectivity, we endeavored to validate whether such structure-property correlations in the hydrogenation of 3-nitrostyrene can be used as a probe reaction to study structure evolution in Pt-Sn systems. During the synthesis of Pt_3Sn iNPs, we initially achieved an alloy phase in TEG solution at 280 °C (denoted as $PtSn_{0.3}$@mSiO$_2$) as shown in Figure S7, and post-annealing in reducing atmosphere at 600 °C is necessary to transition the alloy to the intermetallic phase (denoted as Pt_3Sn@mSiO$_2$). The catalytic performances of fresh alloy ($PtSn_{0.3}$) and

annealed IMC (Pt_3Sn) samples in the hydrogenation of 3-nitrostyrene are different as summarized in Table S2. $PtSn_{0.3}$@$mSiO_2$ NPs show a high selectivity and low activity, while Pt_3Sn iNPs show a decreased selectivity and increased activity. Based on the aforementioned structure-property relationship, the fresh $PtSn_{0.3}$@$mSiO_2$ would likely have an intermetallic PtSn surface, likely due to the lower formation energy of intermetallic PtSn in comparison to Pt_3Sn in the wet TEG synthesis [58]. The annealing treatment can reconstruct the surface of the fresh $PtSn_{0.3}$ to intermetallic Pt_3Sn. To observe this transition of surface composition, we performed an *in situ* AP-XPS on fresh $PtSn_{0.3}$@$mSiO_2$ and annealed it to 500 °C (Figure S8). The fresh $PtSn_{0.3}$@$mSiO_2$ indeed has a Pt/Sn surface ratio (1.33) closer to intermetallic PtSn, largely deviating from their bulk Pt/Sn ratio (3.0), and the annealed Pt_3Sn@$mSiO_2$ presents a matching composition (Pt/Sn = 2.78) to intermetallic Pt_3Sn.

We further extended the intermetallic composition to Zn and Pb as shown in Table 1. For Pt_3Zn@$mSiO_2$, the *cP4* structure of intermetallic Pt_3Zn reflects high activity and poor selectivity, which is similar to their isostructural Pt_3Sn counterpart. All PtM@$mSiO_2$ (M = Sn, Zn, and Pb) demonstrated similar slow rates and high selectivity, indicating similar non-HP reaction mechanism. Intermetallic PtPb has the specific *hP4* unit cell as intermetallic PtSn, and intermetallic PtZn has a *tP2* unit cell. We examined the low index facets including (110), (111), and (100) for PtZn and $(11\bar{2}0)$, $(11\bar{2}1)$ and (0001) for PtPb. No typical Pt threefold site presents in all these facets. The high selectivity of intermetallic PtSn, PtZn, and PtPb commonly corresponds to the absence of Pt threefold sites. In retrospect, the reaction rates follow the trend PtZn<PtPb<PtSn. However, this activity order agrees neither the trend of the atomic radius nor electronegativity (radius: Zn~Pt<Sn<Pb and electronegativity: Zn<Sn<Pt~Pb). These results confer that the geometric effect of IMC structures can more significantly affect the catalytic selectivity in hydrogenation. Nevertheless, the electronic and size effect of IMCs can also alter the activity and selectivity [29], which is challenging to address while providing tremendous research opportunities in future.

4. Conclusion

In summary, we synthesized a series of intermetallic PtM- and Pt_3M-type catalysts (M = Sn, Pb, and Zn). The atomically-ordered intermetallic structures of these catalysts are elaborately correlated to their catalytic properties in the hydrogenation of 3-nitrostyrene. All PtM-type intermetallic compounds show high selectivity to 3-aminostyrene in the hydrogenation of 3-nitrostyrene, in contrast to pure Pt and Pt_3M-type catalysts. Intermetallic PtSn@$mSiO_2$ is also highly selective for the hydrogenation of nitro group in nitroarenes in the presence of bromo, iodo, formyl and methoxy groups. Kinetic studies over Pt, PtSn, and Pt_3Sn revealed that the hydrogenation pathways could be altered due to changes in the surface structure of IMCs. Intermetallic PtSn facilitates a unique non-Horiuti-Polanyi pathway, where the elimination of Pt threefold site inhibits the H_2 dissociative adsorption and, in turn, decreases the reaction rate. DFT calculations and competitive reactions ascribe the high selectivity to the preferential adsorption of nitro groups in 3-nitrostyrene over intermetallic PtSn surfaces. This work demonstrates a molecular engineering of intermetallic structures to tune and elucidate the catalytic mechanism for selective hydrogenations. We anticipate that the geometric effect of IMCs in heterogeneous catalysis can be generalized to instruct the exploration of advanced intermetallic systems for heterogeneous catalysis.

Acknowledgement

This work was partially supported by National Science Foundation (NSF) Grant CHE-1607305. Acknowledgment is also made to the donors of the American Chemical Society Petroleum Research Fund for support of this research on the catalyst synthesis. The theory was supported at Ames Lab by the U.S.

Department of Energy (DOE), Office of Science, Basic Energy Sciences, Materials Science and Engineering Division, under Contract DE-AC02-07CH11358, with additional capabilities made possible from internal Laboratory-Directed R&D (LDRD) funding. We thank Gordon J. Miller for the use of X-ray diffractometer, and Dapeng Jing for the assistance in the XPS measurement.

Reference

[1] K.H.J. Buschow, Rep. Prog. Phys. 40 (1977) 1179-1256.
[2] M. Armbruster, R. Schlogl, Y. Grin, Science and Technology of Advanced Materials 15 (2014).
[3] S. Furukawa, T. Komatsu, ACS Catal. 7 (2017) 735-765.
[4] T.B.L.W. Marinelli, S. Nabuurs, V. Ponec, J. Catal. 151 (1995) 431-438.
[5] F. Delbecq, P. Sautet, J. Catal. 220 (2003) 115-126.
[6] J. Prinz, R. Gaspari, C.A. Pignedoli, J. Vogt, P. Gille, M. Armbruster, H. Brune, O. Groning, D. Passerone, R. Widmer, Angew. Chem. Int. Ed. 51 (2012) 9339-9343.
[7] K. Kovnir, M. Armbruster, D. Teschner, T.V. Venkov, L. Szentmiklosi, F.C. Jentoft, A. Knop-Gericke, Y. Grin, R. Schlogl, Surf. Sci. 603 (2009) 1784-1792.
[8] R.V. Maligal-Ganesh, C. Xiao, T.W. Goh, L.-L. Wang, J. Gustafson, Y. Pei, Z. Qi, D.D. Johnson, S. Zhang, F. Tao, W. Huang, ACS Catal. 6 (2016) 1754-1763.
[9] Y. Pei, R.V. Maligal-Ganesh, C. Xiao, T.W. Goh, K. Brashler, J.A. Gustafson, W. Huang, Nanoscale 7 (2015) 16721-16728.
[10] Z. Qi, C. Xiao, C. Liu, T.W. Goh, L. Zhou, R.V. Maligal-Ganesh, Y. Pei, X. Li, L.A. Curtiss, W. Huang, J. Am. Chem. Soc. 139 (2017) 4762-4768.
[11] A. Burawoy, J.P. Critchley, Tetrahedron 5 (1959) 340-351.
[12] H. Blaser, U. Siegrist, H. Steiner, M. Studer, R. Sheldon, H. van Bekkum, Weinheim: Wiley/VCH (2001) 389.
[13] C.-H. Li, Z.-X. Yu, K.-F. Yao, S.-f. Ji, J. Liang, J. Mole. Catal. A: Chem. 226 (2005) 101-105.
[14] M. Boronat, P. Concepción, A. Corma, S. González, F. Illas, P. Serna, J. Am. Chem. Soc. 129 (2007) 16230-16237.
[15] A. Corma, P. Serna, Science 313 (2006) 332-334.
[16] H. Wei, X. Liu, A. Wang, L. Zhang, B. Qiao, X. Yang, Y. Huang, S. Miao, J. Liu, T. Zhang, Nat. Commun. 5 (2014) 5634.
[17] K.-i. Shimizu, Y. Miyamoto, T. Kawasaki, T. Tanji, Y. Tai, A. Satsuma, J. Phys. Chem. C 113 (2009) 17803-17810.
[18] F. Zhao, Y. Ikushima, M. Arai, J. Catal. 224 (2004) 479-483.
[19] S. Furukawa, K. Takahashi, T. Komatsu, Chem. Sci. 7 (2016) 4476-4484.
[20] S. Furukawa, Y. Yoshida, T. Komatsu, ACS Catal. 4 (2014) 1441-1450.
[21] S. Furukawa, A. Tamura, K. Ozawa, T. Komatsu, Appl. Catal. A 469 (2014) 300-305.
[22] T. Komatsu, D. Satoh, A. Onda, Chem. Commun. (2001) 1080-1081.
[23] T. Komatsu, S.-i. Hyodo, T. Yashima, J. Phys. Chem. B 101 (1997) 5565-5572.
[24] E.W. Zhao, R. Maligal-Ganesh, C. Xiao, T.W. Goh, Z. Qi, Y. Pei, H.E. Hagelin-Weaver, W. Huang, C.R. Bowers, Angew. Chem. Int. Ed. 56 (2017) 3925-3929.
[25] M.T. Paffett, J. Phys. Chem. 94 (1990) 6831-6839.
[26] B.E. Koel, C. Xu, Y. Tsai, -L, Surf. Sci. 385 (1997) 37-59.
[27] P. Samson, A. Nesbitt, B.E. Koel, A. Hodgson, J. Chem. Phys. 109 (1998) 3255-3264.
[28] Y. Shu, H.C. Chan, L. Xie, Z. Shi, Y. Tang, Q. Gao, ChemCatChem DOI: 10.1002/cctc.201700880.
[29] S. Iihama, S. Furukawa, T. Komatsu, ACS Catal. 6 (2016) 742-746.
[30] B. Coq, A. Tijani, F. Figueras, J. Mole. Catal. 71 (1992) 317-333.
[31] X.X. Han, R.X. Zhou, G.H. Lai, B.H. Yue, X.M. Zheng, J. Mole. Catal. A 209 (2004) 83-87.
[32] L. Vitos, A.V. Ruban, H.L. Skriver, J. Kollar, Surf. Sci. 411 (1998) 186-202.
[33] S. Jana, Dalton Trans. 44 (2015) 18692-18717.
[34] K. Lee, M. Kim, H. Kim, J. Mater. Chem. 20 (2010) 3791-3798.
[35] A.U. Nilekar, A.V. Ruban, M. Mavrikakis, Surf. Sci. 603 (2009) 91-96.
[36] H. Rong, J. Mao, P. Xin, D. He, Y. Chen, D. Wang, Z. Niu, Y. Wu, Y. Li, Adv. Mater. 28 (2016) 2540-2546.
[37] X. Wang, L. Altmann, J. Stöver, V. Zielasek, M. Bäumer, K. Al-Shamery, H. Borchert, J. Parisi, J. Kolny-Olesiak, Chem. Mater. 25 (2013) 1400-1407.

[38] D.Y. DeSario, F.J. DiSalvo, Chem. Mater. 26 (2014) 2750-2757.
[39] H.G. Liao, D. Zherebetskyy, H. Xin, C. Czarnik, P. Ercius, H. Elmlund, M. Pan, L.W. Wang, H. Zheng, Science 345 (2014) 916-919.
[40] M. Hoheisel, S. Speller, J. Kuntze, A. Atrei, U. Bardi, W. Heiland, Phys. Rev. B 63 (2001).
[41] L.-C. de Ménorval, A. Chaqroune, B. Coq, F. Figueras, J. Chem. Soc., Faraday Trans. 93 (1997) 3715-3720.
[42] V.R. Stamenkovic, M. Arenz, B.B. Blizanac, P.N. Ross, N.M. Markovic, J. New. Mat. Electrochem. System 7 (2004) 125-132.
[43] C. Dupont, Y. Jugnet, D. Loffreda, J. Am. Chem. Soc. 128 (2006) 9129-9136.
[44] A. Gil, A. Clotet, J.M. Ricart, G. Kresse, M. Garcia-Hernandez, N. Rosch, P. Sautet, Surf. Sci. 530 (2003) 71-86.
[45] A. Hightower, M.D. Perez, B.E. Koel, Surf. Sci. 603 (2009) 455-461.
[46] J. Völter, H. Lieske, J. Catal. 90 (1984) 96-105.
[47] M. Salmeróna, R.J. Gale, G.A. Somorjai, J. Chem. Phys. 70 (1979) 2807.
[48] L. Ma, C.M. Wang, B.Y. Xia, K.K. Mao, J.W. He, X.J. Wu, Y.J. Xiong, X.W. Lou, Angew. Chem. Int. Ed. 54 (2015) 5666-5671.
[49] G. Jerkiewicz, Prog Surf. Sci. 57 (1998) 137-186.
[50] T. Komatsu, S.-i. Hyodo, T. Yashima, J. Phys. Chem. B 101 (1997) 5565-5572.
[51] B. Shi, B.H. Davis, J. Catal. 157 (1995) 626-630.
[52] B. Mattson, W. Foster, J. Greimann, T. Hoette, N. Le, A. Mirich, S. Wankum, A. Cabri, C. Reichenbacher, E. Schwanke, J. Chem. Ed. 90 (2013) 613-619.
[53] B. Yang, X.M. Cao, X.Q. Gong, P. Hu, Phys. Chem. Chem. Phys. 14 (2012) 3741-3745.
[54] B. Bridier, N. López, J. Pérez-Ramírez, J. Catal. 269 (2010) 80-92.
[55] T. Sheng, Y.-J. Qi, X. Lin, P. Hu, S.-G. Sun, W.-F. Lin, Chem. Eng. J. 293 (2016) 337-344.
[56] C. Nikalasson, B. Andersson, N.-H. Schöön, Ind. Eng. Chem. Res. 26 (1987) 1459-1463.
[57] B. Yang, X.Q. Gong, H.F. Wang, X.M. Cao, J.J. Rooney, P. Hu, J. Am. Chem. Soc. 135 (2013) 15244-15250.
[58] X.P. Su, F.C. Yin, M.W. Huang, Z. Li, C.T. Chen, J. Alloys and Compd. 325 (2001) 109-112.